Ion Implantation Damage in SiO_2 Studied with Positron Annihilation Spectroscopy.

By

Marc Spooner

Graduate Program in Physics

Submitted in the partial fulfilment

of the requirements for the degree of

Master of Science.

Faculty of Graduate Studies

The University of Western Ontario

London, Ontario

August 1998

© Marc Spooner 1998

National Library of Canada

Acquisitions and Bibliographic Services

395 Wellington Street
Ottawa ON K1A 0N4
Canada

Bibliothèque nationale du Canada

Acquisitions et services bibliographiques

395, rue Wellington
Ottawa ON K1A 0N4
Canada

Your file Votre référence

Our file Notre référence

The author has granted a non-exclusive licence allowing the National Library of Canada to reproduce, loan, distribute or sell copies of this thesis in microform, paper or electronic formats.

L'auteur a accordé une licence non exclusive permettant à la Bibliothèque nationale du Canada de reproduire, prêter, distribuer ou vendre des copies de cette thèse sous la forme de microfiche/film, de reproduction sur papier ou sur format électronique.

The author retains ownership of the copyright in this thesis. Neither the thesis nor substantial extracts from it may be printed or otherwise reproduced without the author's permission.

L'auteur conserve la propriété du droit d'auteur qui protège cette thèse. Ni la thèse ni des extraits substantiels de celle-ci ne doivent être imprimés ou autrement reproduits sans son autorisation.

0-612-30770-0

Canadä

Abstract

Thermally grown SiO_2 films were implanted with 1.7 MeV silicon ions to fluences of 10^{12}, 10^{13} and 10^{14} ions/cm^2. The resulting damage was studied using a variable energy positron beam. Chemical etching was performed to improve the depth resolution of the technique.

In insulating materials such as SiO_2, ion implantation can cause defects by both the nuclear stopping and the electronic stopping of the implanted ions. The nuclear stopping causes vacancies and displaced atoms. The electronic stopping causes ionization, leading to broken bonds and charged defects.

Analysis of the measured defect profiles, and comparison with TRIM Monte Carlo simulations, allows us to deduce the relative contributions of the nuclear and electronic stopping to the radiation damage, which was nearly constant as a function of depth. It was found that 22% of the predicted vacancies remained after the recombination of defects and that the energy necessary to produce defects by ionization was ~2700 eV/defect.

Keywords: Positrons, SiO_2, electronic stopping, nuclear stopping

Acknowledgements

I would like to express my appreciation to Dr. P. J. Simpson for his guidance during this project. I would also like to thank Dr. U. Myler for many useful discussions.

I thank Dr. H. Xia who performed the ion implantation and helped with the growth of the silicon oxide films, the chemical etching and RBS measurements.

I also would like to thank K. Evans for proof reading this thesis.

Table of Contents

Certificate of Examination ii

Abstract iii

Acknowledgements iv

List of Figures vi

Chapter 1 Introduction 1

Chapter 2 Experimental Techniques 3

- 1. Positron Annihilation Spectroscopy 3
  - a)Positron Interactions with Matter 3
  - b) The University of Western Ontario's Positron Beam 11
- 2. TRIM 15

Chapter 3 Experiment. 19

- 1. Oxide Growth and Ion Implantation 19
- 2. Positron Annihilation Spectroscopy 19
- 3. Increased Depth Resolution 24

Chapter 4 Data Analysis 31

- 1. RBS data 31
- 2. Fitting procedure for Positron Data 33

Chapter 5 Discussion 43

- 1. Types of Defects 43
- 2. Inadequacies of the Fitting Procedure 43

Chapter 6 Conclusions 47

- Future work 48

References 49

Vita 51

List of Figures

2.1 Spectrum of annihilation radiation. 5

2.2 Positron implantation profile. 7

2.3 The University of Western Ontario's magnetically guided slow positron beam 12

2.4 TRIM predictions of the vacancy distribution and energy loss due to ionization produced by the implantation of 1.7 MeV silicon ions into silicon oxide on a silicon substrate. 16

3.1 S parameter as a function of positron implantation energy for silicon oxide films implanted to various fluences of 1.7 MeV silicon ions. 19

3.2 S and R parameters of silicon oxide films as a function of the implanted fluences of 1.7 MeV silicon ions. 20

3.3 Difference spectra of as grown silicon oxide and silicon oxide implanted with 10^{12} Si^{+}/cm^{2}. 22

3.4 S parameter as a function of positron implantation energy of various thicknesses of unimplanted SiO_2 films. 24

3.5 S parameter as a function of positron implantation energy of various thicknesses of SiO_2 films implanted with 10^{12} Si^{+}/cm^{2}. 26

3.6 S parameter as a function of positron implantation energy of a SiO_2 layer grown to 1250Å and a layer grown to 2700Å then etched down to 1250Å. 28

4.1 RBS spectrum of a SiO_2 film on a silicon substrate. 31

4.2 Defect distribution obtained from the positron annihilation spectroscopy measurements. 40

Chapter 1 Introduction

Silicon oxide is a technologically important material for many reasons. It is an insulating material which can easily be formed on silicon to make metal-oxide-semiconductor (MOS) structures. It can be used to form high precision oscillators. It is also used to make optical fibers.

The oxide thickness in MOS structures can be as thin as ~10 nm. As the size of silicon oxide structures get smaller, there is an increased need to understand the effect of defects. Although there have been many studies of defects in SiO_2 (see for example [1,2,3]), the structure of damaged SiO_2 and the SiO_2/Si interface remains incompletely understood. This thesis is a study of the defects produced by the through-oxide-implantation of silicon ions, using positron annihilation spectroscopy (PAS), which is sensitive to vacancy-type defects and to negatively charged defects.

Ion implantation into the silicon through a SiO_2 layer is a possible production method for doping the silicon. As ions are implanted into materials, they slow down due to interactions with both the nuclei and the electrons. Defects may be produced as the ion transfers some of its energy. In the case of the nuclear stopping, the nuclei of the incoming ion and of the atom of the lattice collide, which can lead to displacement of the atom. The displaced atom can

then collide with other atoms causing a damage cascade. This method of defect production has been previously studied thoroughly in semiconductors using positrons [4]. and can be predicted by Monte Carlo simulations such as TRIM [5] The nuclear stopping should have similar effects in insulating materials such as SiO_2.

In insulators, damage can also occur due to the electronic stopping of the ions. This involves ionization in the material, which can lead to broken bonds between atoms as well as subsequent displacements. In metals and semiconductors, the damage done by the electronic stopping is not important because there are enough conduction electrons to replace the electrons lost by ionization. A previous study of ion induced defects in SiO_2 by Knights [6] reported that the defects produced were consistent with a constant defect distribution as a function of depth, which did not agree with the vacancy distribution predicted by TRIM. To explain this, Knights suggested that the electronic stopping plays an important role in defect production.

In this study, the defect distribution is measured with better depth resolution than in any other positron study of silicon oxide, using a combination of positron annihilation spectroscopy and chemical etching. The main objective of this study is to determine the relative contributions of the nuclear and electronic stopping to the resulting defect distribution.

Chapter 2 Experimental Techniques

1. Positron Annihilation Spectroscopy

Positron annihilation spectroscopy involves the implantation of positrons into materials in order to probe for defects. To do this, we use a mono-energetic positron beam. In this section the interactions of positrons with matter are described. Then the observables, and the information extracted from them are discussed. Finally, the experimental setup of the University of Western Ontario's positron beam is described.

a) Positron Interactions with Matter

i) Annihilation

Since the positron and electrons are anti-particles, they can annihilate with each other. During the annihilation, two γ-rays of about 511 keV are emitted in nearly opposite directions. The exact energy and direction of each γ-ray depends on the energy and momentum of the positron and electron at the time of annihilation. The momentum of the positron is negligible (compared to the momentum of the electron) because it has thermalized. Therefore the energy of the emitted γ-rays depends mainly on the momentum of the electron. If the positron annihilates with a high momentum electron, such as a core electron, there can be a large Doppler shift to the annihilation radiation. On the other hand, if the positron annihilates with the lower momentum valence electrons, there will be a smaller Doppler shift.

The amount of Doppler shift of the γ-rays gives an indication of the site of the annihilation. If the annihilation takes place at a vacancy, then the overlap between the wave functions of the positron and the valence electrons is greater than the overlap between the wave functions of the positron and the core electrons. Therefore, the positron is more likely to annihilate with valence electrons. Since valence electrons produce a small Doppler shift, the annihilation radiation from positrons trapped in vacancies will have a small Doppler shift.

To parameterize the γ-ray spectrum, the S parameter is used [8]. The S parameter is defined as the fraction of counts in the central region of the peak, as shown in figure 2.1 . This is thus a measure of the sharpness of the peak. A high S parameter indicates a sharp peak with very little Doppler broadening. In these experiments the central region of the peak is defined as 510.3 to 511.7 keV. The central region is defined in such a way as to produce a parameter as statistically robust as possible, for which we set $S \sim 0.5$. The S parameter is then normalized by dividing it by the S parameter of bulk silicon.

ii) Implantation

The mean depth of the implantation is selected by choosing the positron implantation energy. The distribution of the positrons after implantation can be calculated using Monte Carlo techniques [9] . The results of these calculations

Spectrum of annihilation radiation

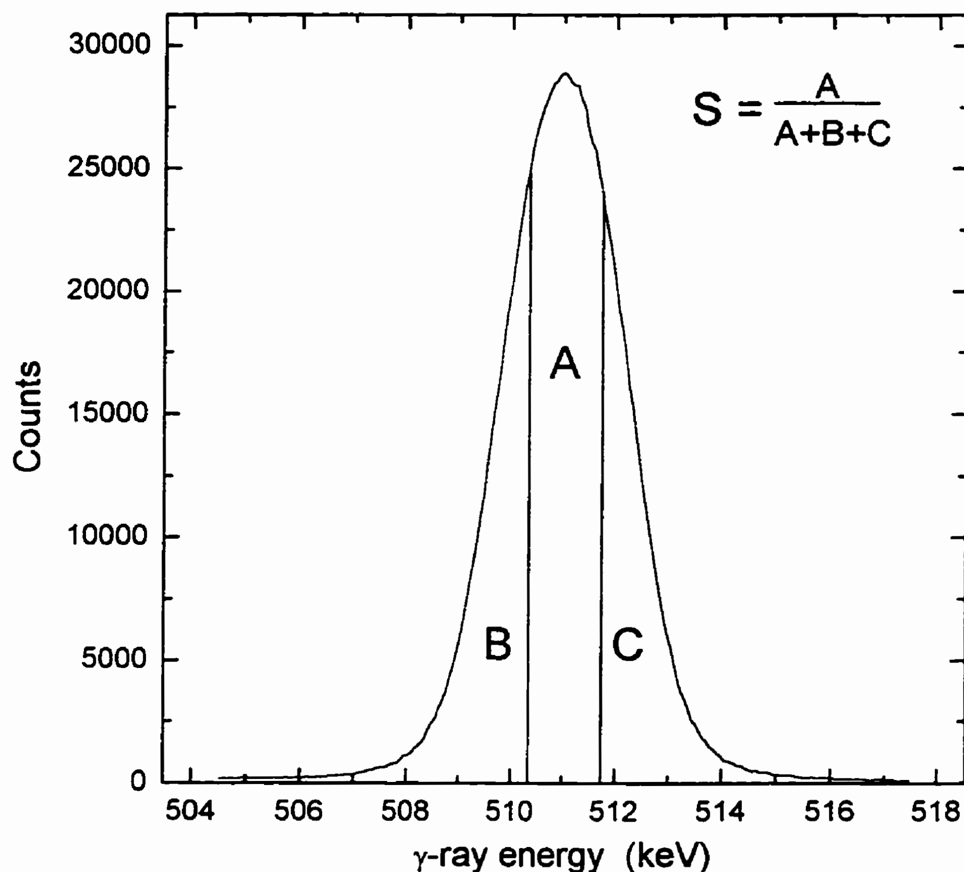

Figure 2.1 Spectrum of annihilation radiation of 5 keV positron implanted into silicon containing 1250000 counts. Also shown is the window used to define the S parameter.

for the implantation profile are often approximated using the Makhovian profile(P(E,z)) with m = 2 :

$$P(E,z) = -\frac{d}{dz}\exp[-(z/z_o)^m] \qquad (1)$$

with

$$z_o = \frac{\bar{z}}{\Gamma(1+1/m)} \qquad (2)$$

and

$$\bar{z} = \frac{A}{\rho}E^n \qquad (3)$$

where E is the positron implantation energy, ρ is the density of the material, $\bar{z}$ is the mean implantation depth and Γ is the gamma function. A and n are material dependant parameters with typical values of 4.00 $\mu g/(cm^2\ keV^{1.6})$ and 1.6 [10].

The depth resolution of positron annihilation spectroscopy is limited by this implantation profile and by positron diffusion after thermalization. Figure 2.2 shows the implantation profile for positron energies of 2 keV and 7keV. This figure shows that as the positrons probe deeper into the sample, the implantation profile is broader, reducing the depth resolution. The mean

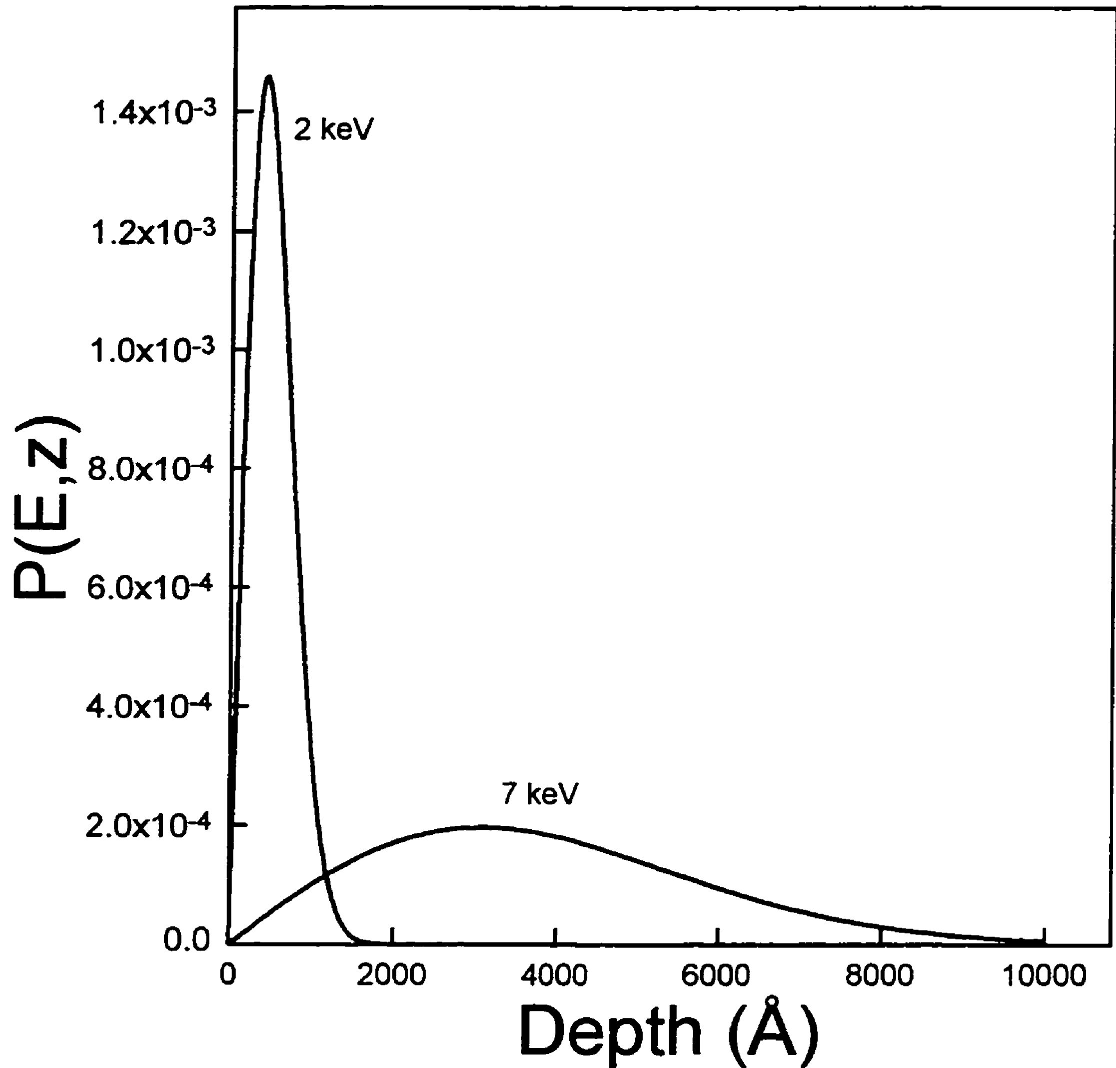

Figure 2.2 The positron implantation profile for 2 and 7 keV positrons into silicon.

depths for these energies are 520 Å and 3860 Å while the full-width-half-maximum (FWHM) of these distributions are 580 Å and 4210 Å, respectively.

iii) Diffusion

After implantation and thermalization, the positrons will diffuse in the sample until they annihilate with an electron, according to the diffusion equation:

$$\frac{\delta n}{\delta t} = D_{+}\frac{\delta^2 n}{\delta z^2} - D_{+}\frac{e}{kT}\frac{\delta[\epsilon(z)n(z)]}{\delta z} - \frac{n(z)}{\tau_{eff}} + \frac{dn_0(z)}{dt} \qquad (4)$$

with

$$\tau_{eff} = \frac{1}{\lambda_{free} + \mu C_d} \qquad (5)$$

where D_{+} is the positron diffusion constant, $\varepsilon(z)$ is the electric field in the sample, k is the Boltzmann constant, T is the temperature, τ_{eff} is the effective time in which the positron is freely diffusing, λ_{free} is the free annihilation rate in the material , μ is the specific trapping rate and C_d is the defect concentration. The last term in equation 4 is the rate at which the positrons thermalize at a depth z and is proportional to the implantation profile P(E,z) . Once a steady state solution is obtained, the term $\delta n/\delta t = 0$ and equation 4 simplifies to:

$$\frac{d^2n(z)}{dz^2} - \frac{e\epsilon}{kT}\frac{dn(z)}{dz} - \frac{n(z)}{D_+\tau_{eff}} + \frac{dn_o(z)}{D_+\,dt} = 0 \qquad (6)$$

iv) Trapping

A vacancy consists of the absence of a positive ion core at a lattice site. For positrons, the potential at the vacancy is at a minimum [11]. The positron can become trapped at the minimum of the potential well (ie. at the vacancy) and provided that the potential well depth is much greater then kT, the positron will stay trapped until it annihilates with an electron. This type of trapping can also occur at divacancies, voids and negatively charged defects.

Positrons are a sensitive probe for defects because they are easily trapped by vacancy-like defects. The smallest change observable for the S parameter is about 0.001 . In silicon this corresponds to a 5% change in the fraction annihilating at defects. The sensitivity to defects is limited to concentrations trapping between ~5 and ~95% of the positrons which correspond to defect concentrations of $\sim 4\times10^{16}$ to $\sim 1.5\times10^{19}$ defects/cm^3 [4].

Saturation in positron trapping occurs when more than 95% of the positrons are trapped at defects. Increasing the number of defects cannot significantly increase the fraction of positrons trapped. Samples with a large concentration of defects have an S parameter characteristic of the defect.

v) Positronium Formation

Before annihilation, it is possible for a positron and an electron to form positronium in both large open voids, and at the surface of materials. This is an electron-positron bound state similar to a hydrogen atom with the proton replaced by a positron. 75% of the positronium formed will be ortho-positronium , the triplet state (L = 1) and 25% will be para-positronium, the singlet state (L = 0). The singlet state will annihilate by the usual 2 γ-ray mechanism as discussed previously. The triplet state may annihilate via a 3 γ-ray mechanism where all three γ-rays have energies lower then 511 keV. It is also possible that the positron annihilates by pick-off, with an electron other than the one to which it is bound, emitting 2 γ-rays.

The R parameter is defined as the ratio of the number of detected γ-rays with energy below the annihilation peak at 511 keV to the total number of γ-rays detected, i.e.

$$R=\frac{T-P}{P} \qquad (7)$$

where T is the total number of counts in the spectrum and P is the number of counts in the peak. The peak is defined as the region from 490 to 527 keV, and to minimize the effect of scattered radiation, the 'total' spectrum is only taken from 360 to 527 keV. The amount of positronium formation can be estimated using the R parameter. Since the predominant source of γ-rays

with energies between 490 and 360 keV are from the annihilation of ortho-positronium, the number of these of counts is a measure of the amount of ortho-positronium annihilations.

Because of the possibility of pick-off, the R parameter only sets a lower limit to the amount of para-positronium formation. Using the ortho-positronium to para-positronium formation ratio of 3:1, this also sets a lower limit to the amount of positronium formation.

b) The University of Western Ontario's Positron Beam

The experimental setup is shown in figure 2.3 . While operating, the pressure in the chambers is typically a few $\times 10^{-7}$ torr. This is necessary to make the mean free path large compared to the distance between the source and the sample under investigation.

The positron beam is roughly circular with a diameter, of about 0.5 cm, which varies with the energy of the beam.

i) Source

The positrons used in these experiments come from the β^+ decay of a ~ 35 mCi (as of July 20 1998) ^{22}Na source located in the source chamber. These are fast positrons with energies ranging from 0 to 546 keV. ^{22}Na is used as a

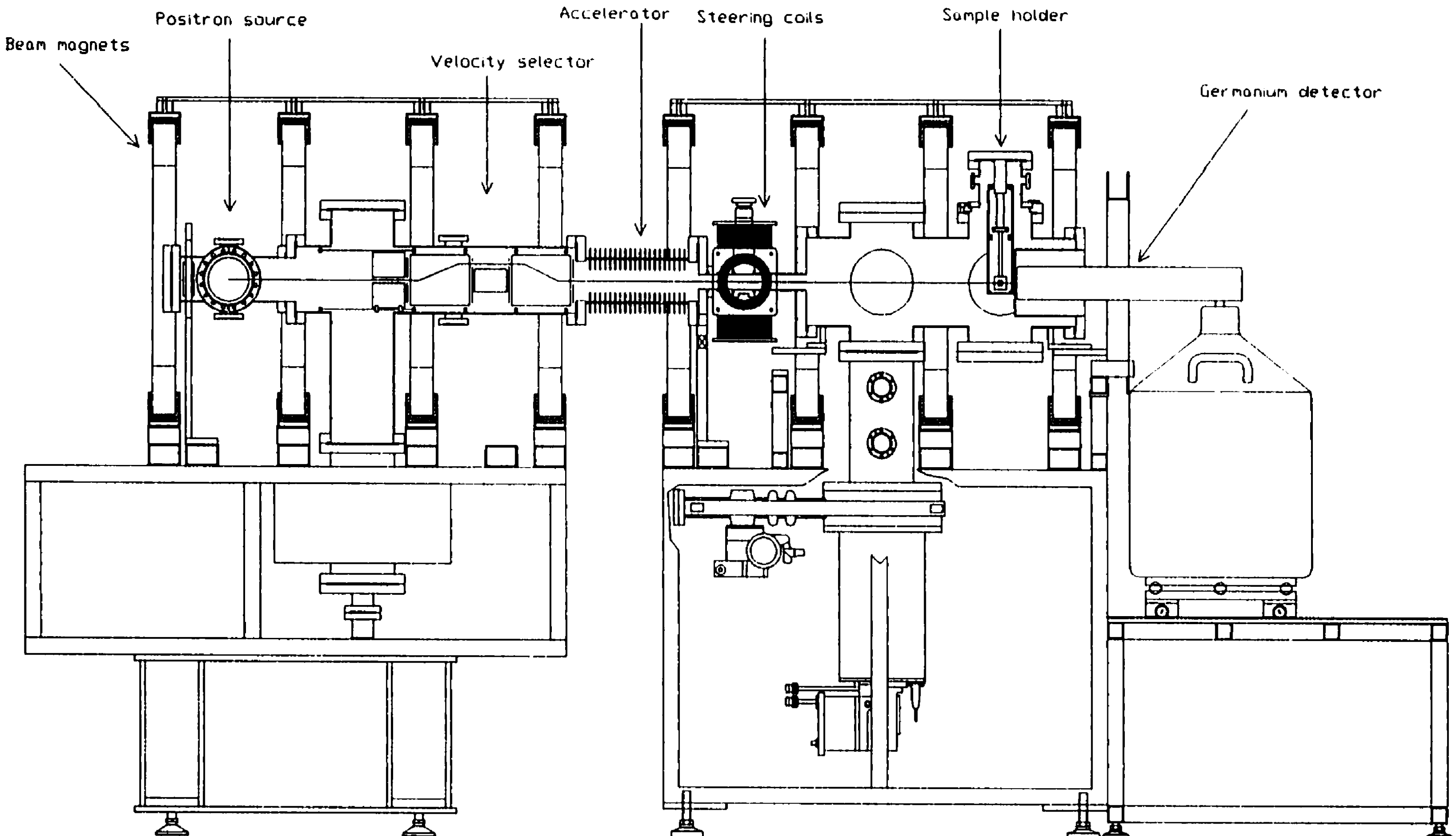

Figure 2.3 The University of Western Ontario's magnetically guided slow positron beam [5].

source because of its relatively long half-life (~2.6 years).

ii) Moderator

These fast positrons have a large velocity distribution and must be moderated in order to produce a mono-energetic positron beam. A 1 μm thick tungsten film placed near the source is used as a moderator. Most of the positrons pass through the moderator, but some of the positrons thermalize and are then emitted from the surface.

Positrons in tungsten have a negative work function. This means that it is energetically favourable for the positrons to be in the vacuum instead of in the tungsten. As a result of this when thermalized positrons get near the surface of the tungsten, they are emitted with an energy equal to the work function ~3 eV with a full width at half maximum of ~ 75 meV [12].

iii) Velocity Selector

The slow positrons need to be separated from the fast positrons that have gone through the tungsten moderator without thermalizing. This is done with a $\vec{E} \times \vec{B}$ filter. The positrons go through an electric and magnetic field such that only the slow positrons are deflected enough to pass through the apertures in the $\vec{E} \times \vec{B}$ plates. The fast positrons hit the plates, and a tungsten brick located just behind the plates stops the γ-rays from annihilations at the source, in the

moderator and at the $\vec{E} \times \vec{B}$ plates.

iv) Accelerator

The positrons that get through the $\vec{E} \times \vec{B}$ filter are then accelerated using an electric field. The source end of the beam including the source, is at a high positive voltage, while the target end is at ground potential. The accelerator is a series of 20 electrodes separated by ceramic rings, with equal-valued resistors between successive electrodes. The energy of the positrons can be selected by varying the voltage of the source. Positron energies of 550 eV to 60 keV can be obtained using this apparatus.

v) Focussing and Targeting

The beam is guided towards the target by a ~100 Gauss magnetic field generated by large solenoids around the chambers. If the positron travelling with a velocity v is not going parallel to the magnetic field B, the resulting force $\vec{F}$ will be:

$$\vec{F} = e\,\vec{v} \times \vec{B} \qquad (8)$$

This will make the positron spiral around the field lines with a radius

$$R = m_e v_\perp / eB \qquad (9)$$

where m_e is the mass of the positron, $v_\perp$ is the component of the velocity perpendicular to the magnetic field, e is the charge of the positron and B is the magnitude of the magnetic field. Minor adjustments to the path of the

beam are made using the magnetic fields of 4 small steering coils.

vi) Data Acquisition

After the positrons annihilate in the sample, the γ-rays are detected using a germanium detector. At 511keV, the energy resolution of the germanium detector is 1.3keV. The output of the germanium detector is amplified then sent to 2 single channel analyzers and a multi channel analyzer. The single channel analyzers count the number of events in the peak, and in the total γ-ray spectrum, for calculation of the R parameter. The multichannel analyzer collects the γ-ray spectrum in 197 channels, 66 eV wide between 504.5 and 517.5 keV. The γ-ray spectrum is stored on a computer which also calculates the S parameter.

2. TRIM

TRIM is a Monte Carlo based simulation program for the Transport of Ions in Matter. This was used to help predict the defect distribution caused by ion implantation. The results of these calculations for 1.7 MeV Si ions into a 1.16μm SiO_2 overlayer on a silicon substrate are shown in figure 2.4. This vacancy distribution is the damage produced by the collision between the ion and the nuclei of the material.

In previous positron studies, it has been found that the defect distribution in

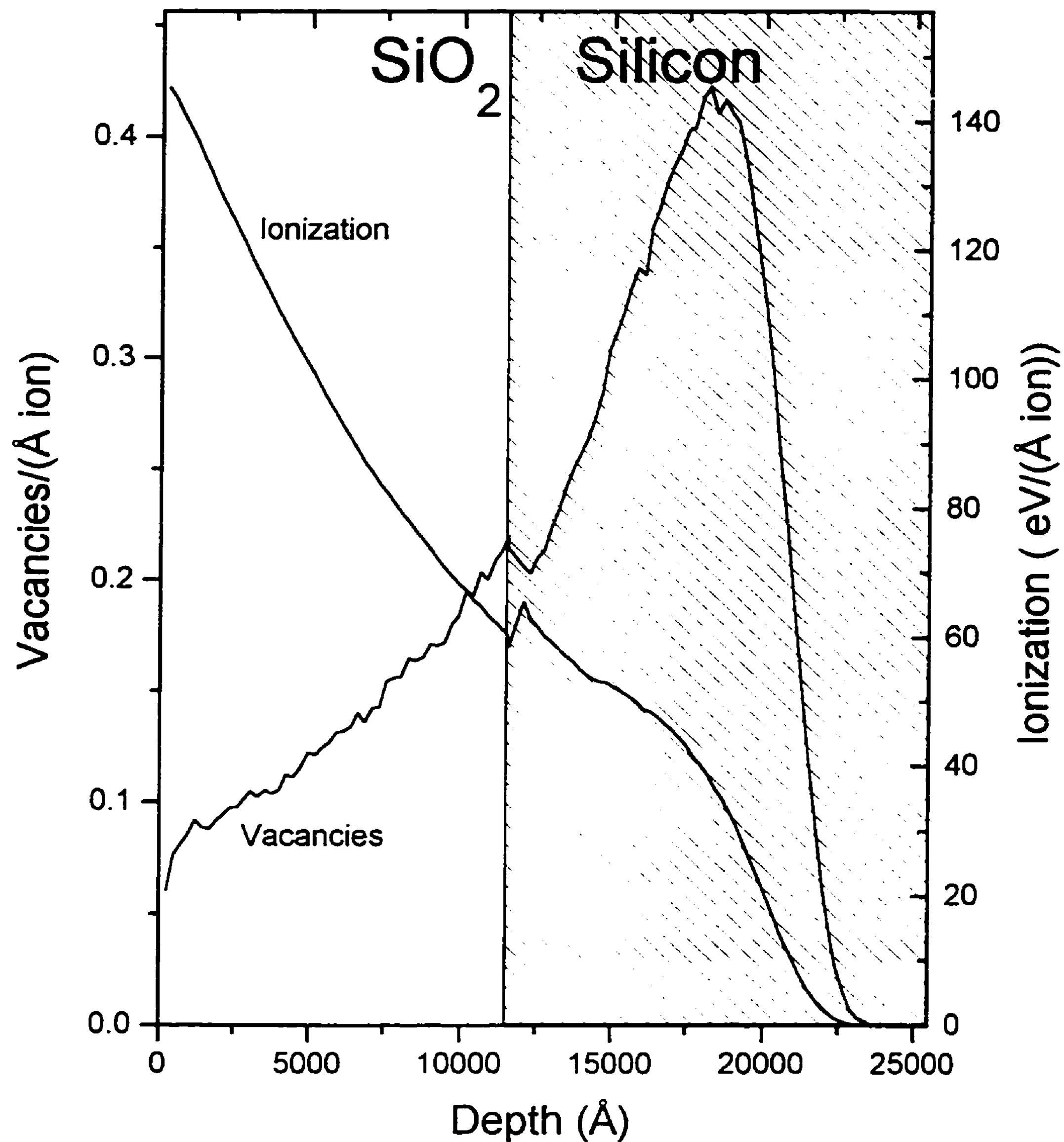

Figure 2.4 TRIM prediction for the distribution of the vacancies produced by the nuclear stopping and the distribution of the energy loss due to ionization for 1.7 MeV Si^+ implanted into a 1.16 um SiO_2 layer on a silicon substrate .

silicon is proportional to the vacancy profile predicted by TRIM [4]. Recombination between the ejected nuclei and a vacancy is then possible but this is not considered by TRIM. This recombination is responsible for the fact that the number of vacancies determined experimentally is about an order of magnitude lower than the number of vacancies predicted by TRIM.

As will be discussed later, the TRIM vacancy distribution does not adequately describe well the experimentally determined defect distribution in the SiO_2 layer. Other sources of defects must be considered to explain the resulting defect distribution. Another possible source of defects is the electronic stopping. This has not been found to be an important factor in the production of defects in metals and semiconductors. This may be due to the fact that metals and semiconductors have conduction electrons, which are able to replace the electron removed by ionization. Because of the higher charge mobility in metals and semiconductors, any charged defects can be effectively repaired or screened. In insulating materials, there are no conduction electrons to repair or screen defects.

It is reasonable to assume that some damage will result from the electronic stopping of the ions because: 1) the electronic stopping accounts for 82% of the energy loss of the implanted ion and 2) that defects in SiO_2 can be produced by ionizing radiation such as 5.0 eV photons [13] or 300-1000 eV

X-rays [14] . Assuming that the defects produced by the electronic stopping do not interact with each other, the number of defects produced would be proportional to the energy loss due to ionization. TRIM can predict the distribution of energy loss due to ionization, and the results are shown in figure 2.4.

With these assumptions, the resulting defect distribution will be:

$$D(z) = aV(z) + bI(z) \qquad (10)$$

where $D(z)$ is the resulting defect distribution, $V(z)$ and $I(z)$ are the distributions of vacancies and energy loss due to ionization and a and b are constants to be determined.

Chapter 3 Experiment

a) Oxide Growth and Implantation

The starting material was a wafer of FZ <100> silicon, p-type, boron-doped, with a resistivity of 10.4 Ω·cm. A 1.16 μm silicon oxide layer on the silicon substrate was produced by heating it to 1200 °C for 24 hours under constant water vapour flow. The wafer was then cut into 4 pieces, 3 of which were implanted with 1.7 MeV silicon ions using the University of Western Ontario's Tandetron accelerator. The samples were implanted to fluences of 10^{12} , 10^{13} and 10^{14} Si^{+}/cm^{2}.

b) Positron Annihilation Spectroscopy Results

The samples were then studied using positron annihilation spectroscopy. In figure 3.1, the S parameter as a function of the positron implantation energy is shown for samples receiving different fluences of Si ions. The mean depth, probed by the positrons, is indicated on the top axis. The shaded part of the graph represents the silicon substrate. The S parameter of the silicon oxide is reduced by the ion implantation induced defects. There is a much larger difference between the samples implanted with 10^{12} and 10^{13} ions/cm^{2} than there is between the samples implanted with 10^{13} and 10^{14} ions/cm^{2}. This is because, around 10^{13} ions/cm^{2}, the fraction of positrons trapped in defects is approaching saturation.

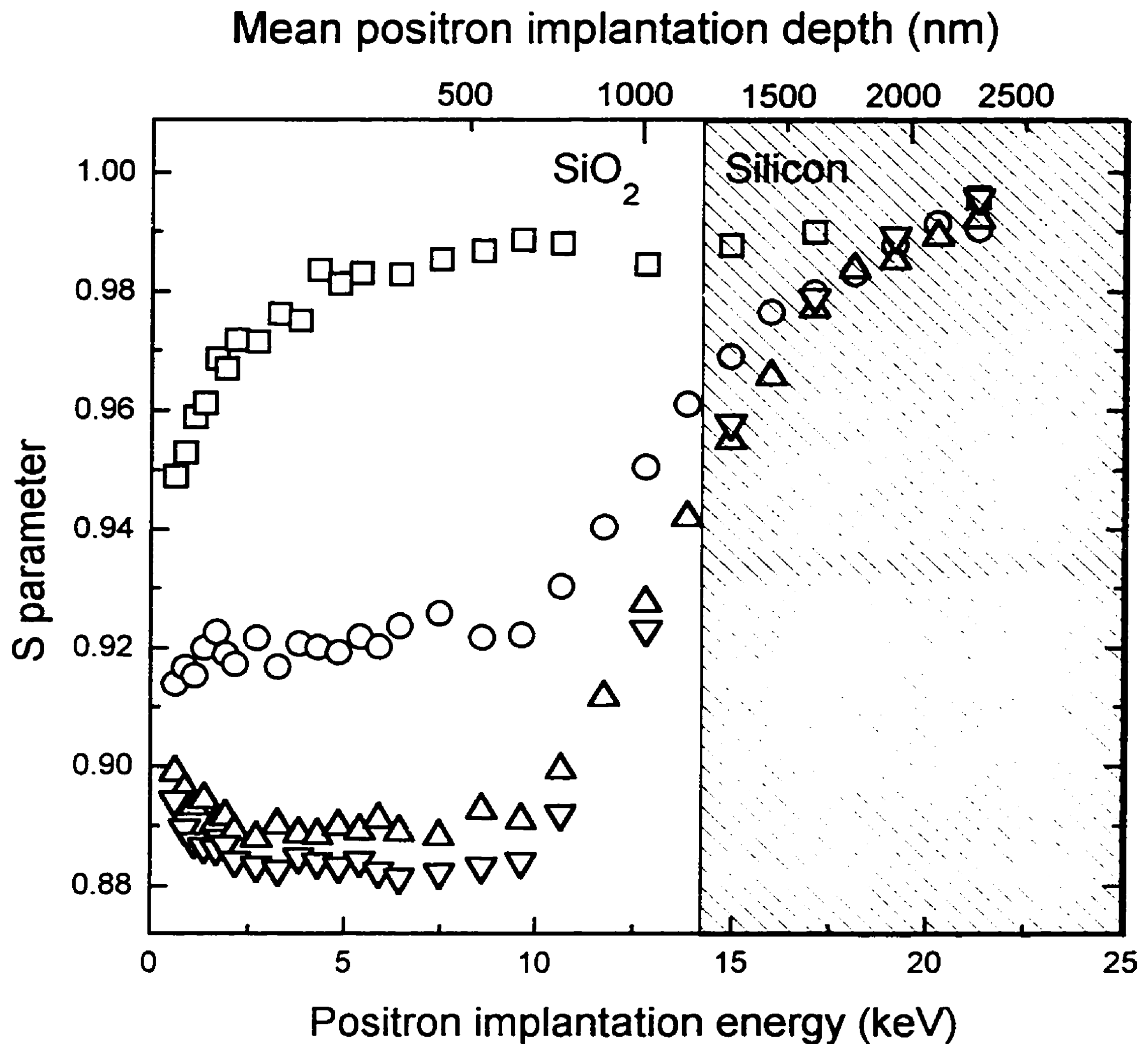

Figure 3.1 . S parameter as a function of positron implantation energy for the sample as grown(□), and samples implanted with 10^{12} (○) ,10^{13} (△) and 10^{14} (▽) Si^{+}/cm^{2}.

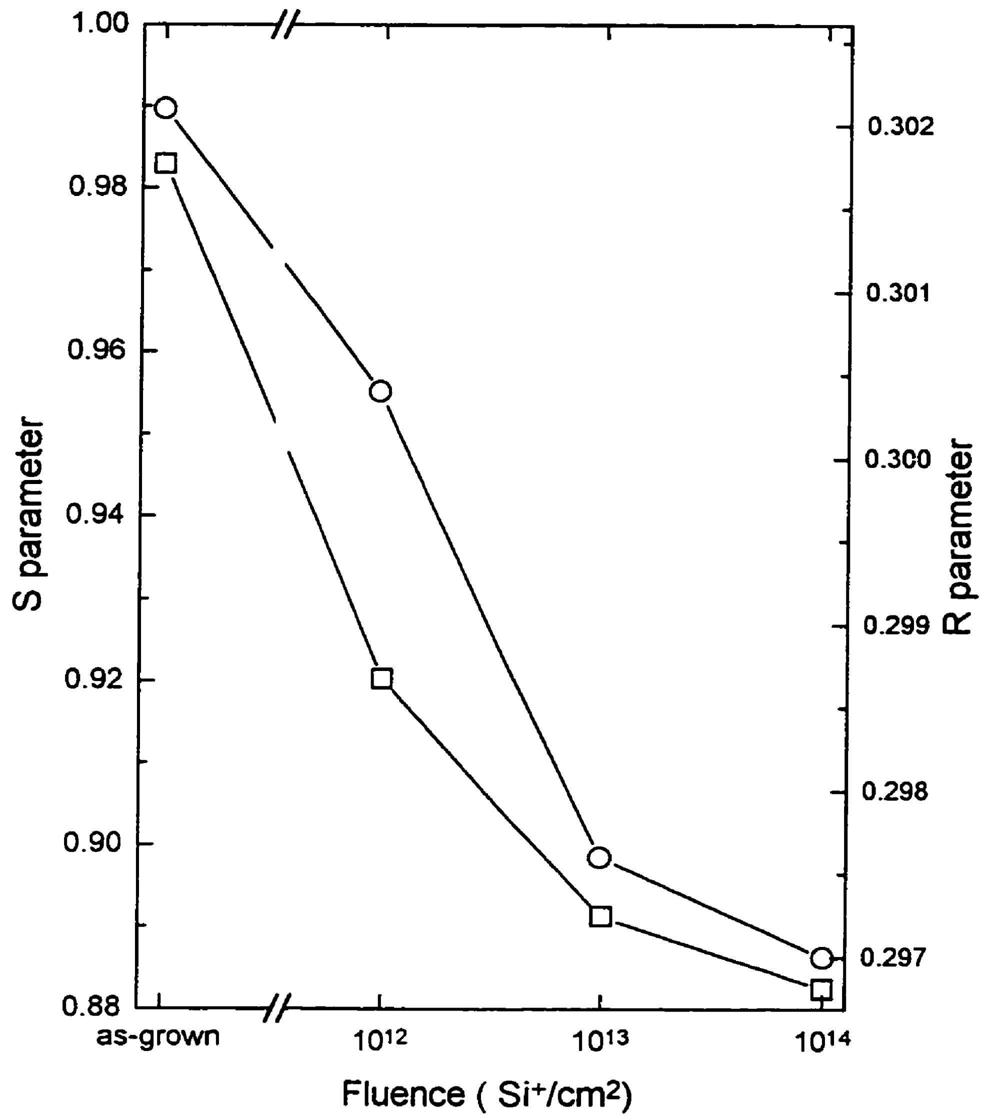

Figure 3.2 . S (o) and R (□) parameters as a function of the fluence of the1.7 MeV Si^+ implant into SiO_2.

In figure 3.2, the S and R parameters of the SiO_2 layer are plotted as a function of the implanted fluence. The S parameter used in this figure is the S parameter obtained for a positron implantation energy of 6.5 keV. To get statistically significant values, the R parameter was obtained by averaging the values of R between 5 and 11 keV. The effect of the ion induced defects is to reduce the S and R parameters. The lower R parameter indicates that less positronium is being formed in the implanted samples. The simultaneous drop in S and R is an indication that the reduction in the S parameter may be due to a reduction in positronium formation.

To be certain of this, it is necessary to examine the positron annihilation spectra more closely. To emphasize the differences between spectra, difference spectra are used which are plotted in figure 3.3 . The difference spectra are obtained by subtracting from the data, a reference spectrum, in this case the spectrum of bulk silicon. In the difference spectrum of the unimplanted silicon dioxide, there is a narrow peak centred at 511 keV and a pair of peaks in the "wings". The momentum of positronium is low, therefore the annihilation of positronium produces a very sharp peak such as the central peak observed in the difference spectrum. The peaks, at 509 and 513 keV, have been shown to be characteristic of oxygen [15].

The difference spectrum of the implanted sample looks similar to the

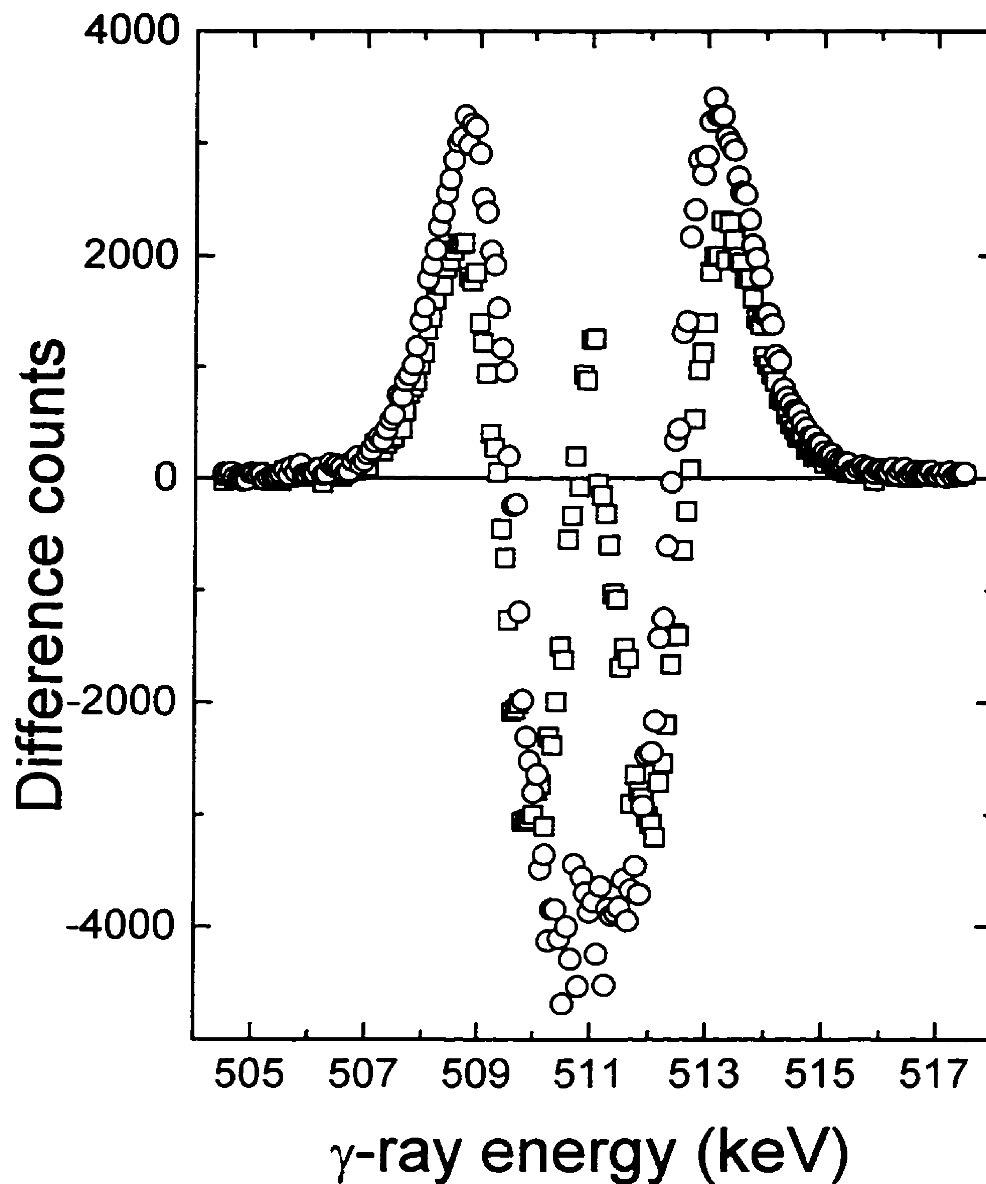

Figure 3.3 Difference spectra obtained by substracting the spectrum of silicon from the spectrum of thermally grown SiO_2, as-grown(□) and implanted with 10^{12} Si^{+}/cm^{2} (o) . Each spectrum contains $2x10^{6}$ counts.

unimplanted spectrum, with the exception that the narrow central peak is missing, therefore less positrons are forming positronium before annihilating. The defects suppress positronium formation by trapping the positrons before they can enter the voids where positronium formation is possible. The absence of the narrow component will cause the γ-ray spectrum to be broader, reducing the S parameter.

c) Increased Depth Resolution

To improve the depth resolution when probing deep into the sample, a combination of positron measurements and chemical etching was used on the unimplanted sample and the sample implanted with 10^{12} Si^+/cm^2. The samples were measured, then 120 nm of oxide was removed by chemical etching using a 5% HF solution. The samples were measured again, then more oxide was etched away, and so on, until we progressed through the entire SiO_2 layer. The first etch removed 120 nm of oxide while all subsequent etches removed 150 nm of oxide. In this way each part of the SiO_2 layer was measured at least once when it was less then 150 nm from the surface. This procedure also put strict constraints on the fitting parameters since the models used to fit the data must all be consistent.

The results of the measurements are shown in figure 3.3 for the unimplanted sample. Only 4 sets of data are shown for clarity. All the curves have a low S

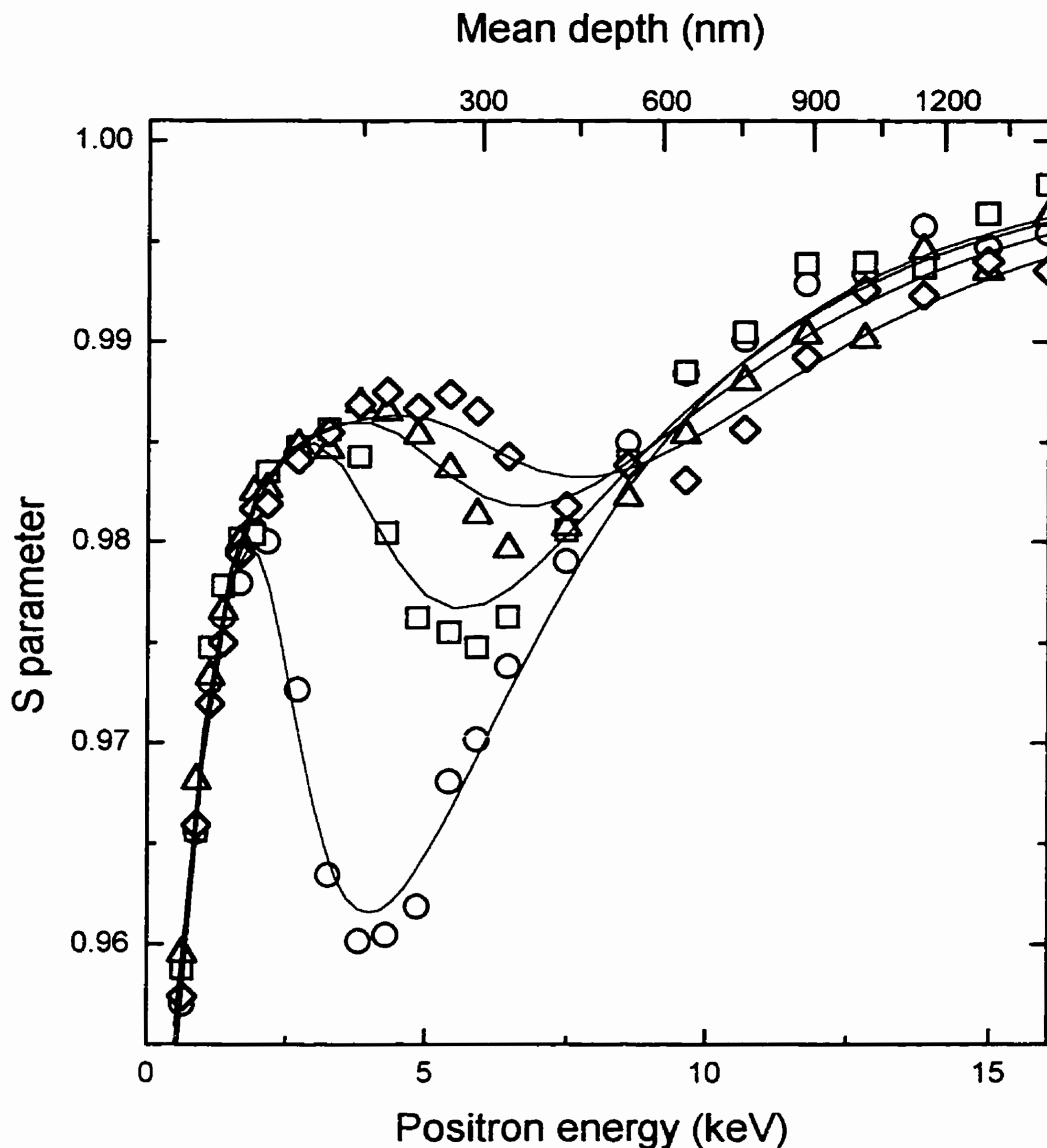

Figure 3.4 . S parameter as a function of positron implantation energy for a SiO_2 layer with various thicknesses on a silicon substrate. The remaining SiO_2 thickness was 113nm (○), 236nm (□), 357nm (△) and 483nm(◇). The lines represent the fits to the data.

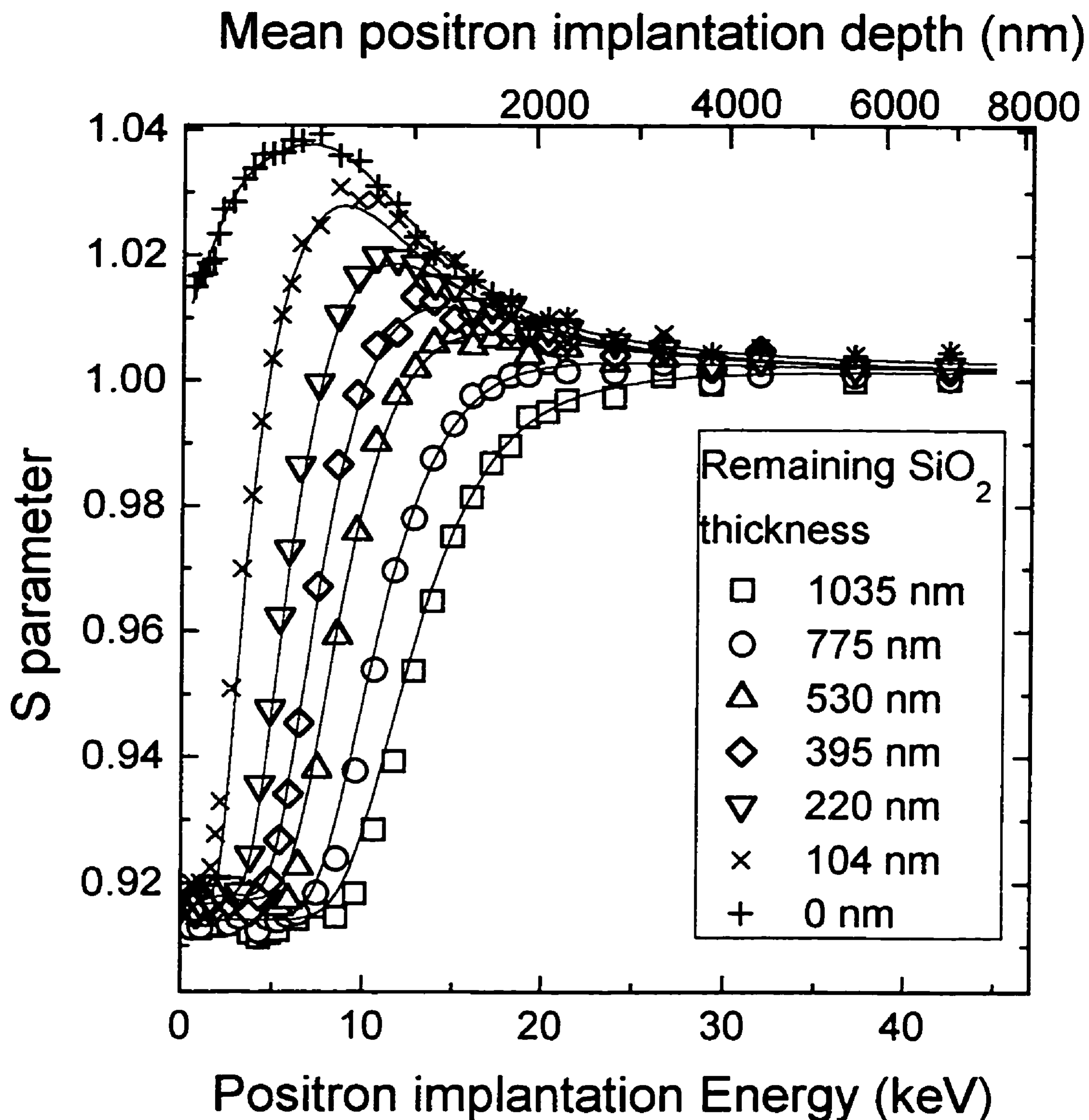

Figure 3.5 . S parameter as a function of positron implantation energy for a SiO_2 on a silicon substrate implanted with 10^{12} Si^+/cm^2. The SiO_2 was etched to various thicknesses after implantation. The lines represent the fit to the data.

parameter near the surface, which increases as the positrons probe deeper into the SiO_2 layer. As the positron mean depth approaches the position of the interface, there is a decrease in the S parameter. As the positrons are implanted past the interface, all the curves converge to a S parameter of 1.00 which occurs at an energy of about 30 keV (not shown). Notice that the interface signal (the dip in the curve) becomes much more apparent when the interface lies closer to the surface.

Figure 3.4 represent the measurements of the S vs.E curves for the sample implanted with 10^{12} Si^+/cm^2 with various amounts of SiO_2 remaining. All of the curves have the same nearly constant S value for depths corresponding to the SiO_2 layer. This suggests that the defect distribution within the SiO_2 is nearly constant.

The TRIM defect profile (figure 2.4) shows that the vacancies produced by the nuclear stopping extend beyond the SiO_2 layer into the silicon substrate. With a thick oxide, the observation of these defects is impossible, but with the removal of some oxide by chemical etching, the defects in the silicon substrate become more evident.

In silicon, the defects cause the S parameter to increase. The defects in silicon are mostly divacancies. When a positron is trapped in a vacancy-type

defect, it will be further from the core electrons, and will annihilate primarily with the lower momentum valence electrons. There will be less Doppler shift, and thus the peak will be narrower and S will be higher.

Any measurement of S parameters higher than 1 clearly indicates defects in the silicon substrate. Looking at figure 3.5 , all the curves with 530 nm of SiO_2 or more show that the S parameter rises above 1, thus the ion induced defects can be observed in the silicon when there is an SiO_2 overlayer as thick as ~530 nm. The thickness of film in which the defects can be observed will however depend on the amount of damage produced.

To test whether the HF etching has an effect on the sample, other than removal of the SiO_2 layer, a sample grown with a thin SiO_2 layer was compared to a sample that had a SiO_2 layer etched down to the same thickness. The thin layer of SiO_2 was grown on a silicon substrate by heating a piece of silicon to 1150°C for 0.5 hour. This was compared to a sample which was grown at 1150°C for 2 hours, then etched to the same thickness as the previous sample. The thicknesses of the samples were found to be 1250 Å and 2700 Å by RBS.

The thicker sample was etched using a 5% HF solution for 242 seconds, reducing its thickness to 1250 Å. Both samples were measured with PAS

and the results are shown in figure 3.6 . The minimum of the S vs. E curves is due to the interface. For the unetched sample, the S parameter at the minimum is slightly lower, but this may be due to a slightly thinner SiO_2 layer. It is clear that there is no drastic reduction in the S parameter due to etching of the sample.

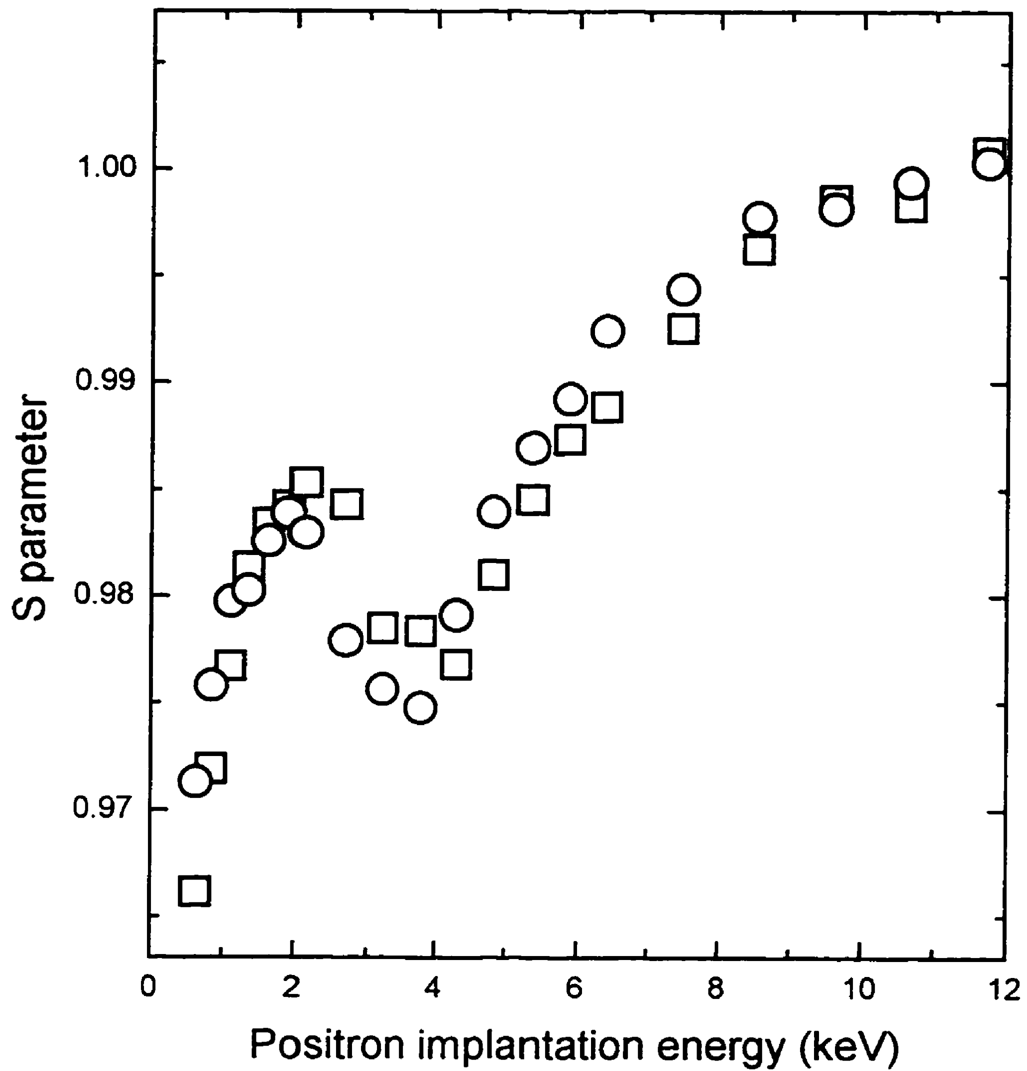

Figure 3.6 S parameter as a function of positron implantation energy for a SiO_2 layer grown to 1250Å on a silicon substrate(O) and a 2700Å SiO_2 layer etched down to 1250 Å (□).

Chapter 4 Data Analysis

1.RBS data

The thicknesses of the SiO_2 layers were determined using RBS. A typical RBS spectrum of a SiO_2 layer on a silicon substrate is shown in figure 4.1 . This spectrum was obtained using a 1 MeV $^4He^+$ beam with the detector placed at an angle of 150° from the beam. The features of this spectrum are (reading the graph from right to left) the onset of the silicon signal at the surface, an increase in the silicon signal at the SiO_2/Si interface, and an oxygen peak. The increase in the silicon signal at the SiO_2/Si interface is due to the increase in silicon concentration. The oxygen peak is at lower energies because oxygen is lighter and more energy is transferred to the recoiling oxygen atom, leaving less energy for the backscattered ion.

The thickness of the SiO_2 layer can be determined in two ways: 1) by the difference in energies between the onset of the Si signal from the SiO_2 and from the silicon substrate and 2) by looking at the width of the oxygen peak. Both these features should indicate the same width. To calibrate the measurements, a sample consisting of Bi implanted silicon was used. The Bi profile extended to a depth of 260 Å.

The thickness of the as-grown sample was found to be 1.16±0.06 μm. The thickness was measured after each etch. The etch rate was constant within

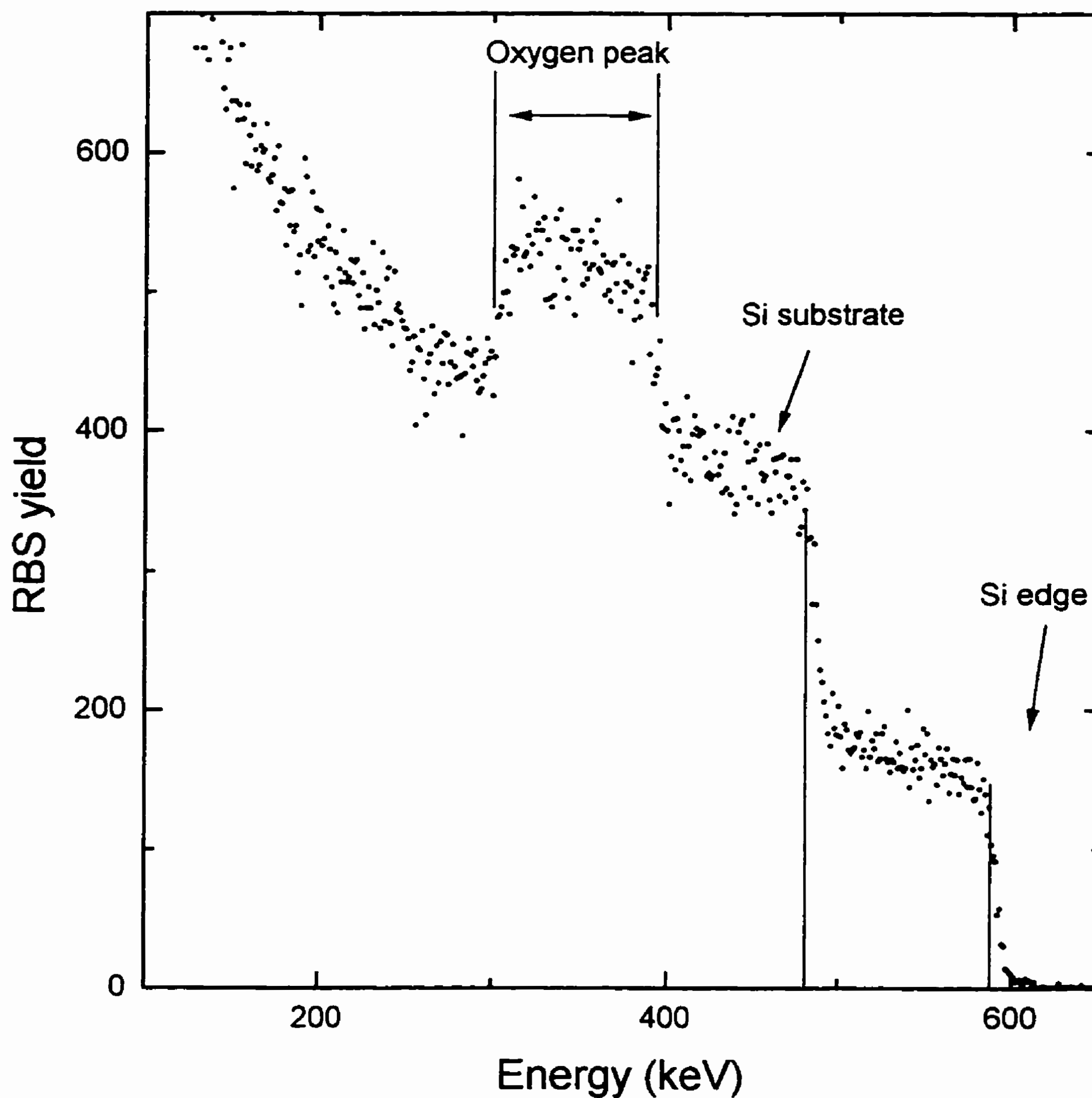

Figure 4.1 . Rutherford backscattering spectrum of a SiO_2 layer on a silicon substrate. The spectrum was obtained using 1 MeV He ions.

the uncertainty of the measurement and found to be 5.8±0.3 Å/s.

2. Fitting Procedure for Positron Data

To fit the data, a model is supplied to the computer program POSTRAP5 [16] describing the sample structure. The sample can consist of a number of regions, each with its own defect concentration, positron diffusion constant, free annihilation rate and positron trapping rate of its defects. The program solves the diffusion-annihilation equation (equation 5) by further dividing the regions into thin layers and approximating the positron implantation profile ($P(E,z)$) to be a second order polynomial in each layer, making the solution analytical.

This program calculates the fraction of positrons annihilating in each state. The surface is considered to be an efficient trap for positrons, therefore any positrons diffusing back to the surface are considered to annihilate in the surface state. The program also calculates the fraction of positrons annihilating, free and trapped, for each region defined in the model. The output of the program is a list of the fractions of positrons annihilating in each state, for a range of positron implantation energies.

The next step is to assign an S parameter for each of the possible states. The experimental data is modeled with the program SFIT5. This fits the data with:

$S(E) = \Sigma f_i(E)S_i$ (11)

where S(E) is the measured S parameter as a function of the positron energy, $f_i(E)$ is the fraction of positrons annihilating in state i and S_i is the S parameter of state i. The program can use the values of S_i as fitting parameters, allowing them to either vary or to be fixed to a certain value.

Fitting the data consists of suggesting a model, comparing the data with the result of SFIT5, then adjusting the model until there is good agreement between the two.

The models for the unimplanted sample were divided into 2 regions (the SiO_2 and the interface) plus the substrate. The thickness of the SiO_2 regions was determined by varying them until a good fit to the S parameter data was obtained. The thicknesses of the SiO_2 layer necessary to fit the data were consistent with the RBS measurements.

a) SiO_2/Si interface

The interface is very efficient in trapping positrons. The interface was modeled as a 50 Å layer with enough defects to trap all of the positrons that are implanted or diffuse into it. 50 Å was chosen to ensure that no positrons can diffuse through it.

The interface has a significant effect on the data for the unimplanted samples. The dip in the S vs. E curves is produced by the interface which has a lower S parameter than both SiO_2 and silicon. The position of the interface is determined by iteratively guessing it, then running the fitting program. If the interface is not deep enough, the dip in the model data will be at a lower energy then the dip in the experimental data. The value of the S parameter assigned to the interface can be determined by adjusting it to give the correct depth to the dip in the data.

For the implanted samples, the position of the interface is less obvious. The reason for this is that the S parameter of the interface is in between the S parameters of the damaged SiO_2 and of silicon. Assuming that the S parameter of the interface is the same as for the unimplanted sample, the interface position can be determined. There is, however, a strong interdependence between the S parameter of the interface and the interface position (ie. having a value too high for the S parameter of the interface will produce an adequate fit if the interface position is too deep) .

b) Defects in Si

The shape of the defect profile in the silicon was assumed to be proportional to the vacancy distribution predicted by TRIM. This has been experimentally verified by Simpson et. al. [4]. The reason that only the shape, and not the

absolute defect concentration, is used is that some of the interstitial atoms recombine with the vacancies, and this process is not modelled by TRIM . The defect distribution is approximated in the model by 3 regions of constant defect concentration as shown in figure 4.2 .

c) Defects in SiO_2

The defect profile in the SiO_2 was determined by fitting the data. The defect concentrations for the thinnest SiO_2 layers were determined first, then used in the models for measurements with thicker oxides. The defect concentration for a region of the sample was always determined from data obtained when that region was about 1500 Å from the surface. For example: the defect concentration of the sample after 8 etches was determined first. This defect concentration was then used as the defect concentration of the deepest 1060 Å of SiO_2 in the sample with 7 etches. The defect concentration for the remainder of the SiO_2 could then be optimised. In this way, it is only necessary to deduce the defect concentration of the 1500 Å of SiO_2 closest to the surface. Thus the degradation of resolution with depth is avoided, and consistency between models is ensured.

d) S Parameters

i) Parameter of the Silicon Substrate

In this case, the S parameter of the substrate corresponds to the S parameter

obtained when all of the positrons annihilate in defect-free silicon. One way of obtaining this result is by measuring the S parameter of a piece of the virgin silicon sample used to grow the oxide. This measurement should have only 2 contributions: the surface and the undefected silicon. Fitting the data with such a model gives an S parameter of silicon for 0.5088 (or 1.00 normalised) .

This value can also be estimated using results from the samples with an SiO_2 film. If the positron implantation energy is sufficiently large, the fraction of positrons diffusing back to the surface will be negligible. The average value of S for high values of E is 0.5096 (or 1.0016). All of the S vs. E curves converge to the same S value for high positron implantation energies. This is because, for these energies, the positrons are implanted deep in the sample and the fractions annihilating at the surface, in the SiO_2 or in the damaged Si region, are negligible.

ii) Surface S Parameter

It was impossible to fit the data using a consistent value for the S parameter of the surface. This is not an unusual result as the surface S parameter is very sensitive to the concentration of impurities such as H or H_2O. In all of the fits, the surface S parameter was allowed to vary freely.

iii) S Parameter of SiO_2

The S parameter of undefected SiO_2 is a fitting parameter that can be estimated by looking at the S vs. E curves of one of the samples with a reasonably thick oxide . In the region where the curve is flat, the positrons are implanted deeply enough to stay within the SiO_2 layer, but not deeply enough to reach the SiO_2 interface. The level of this plateau gives a good indication of the value of the S parameter for the undamaged SiO_2. The S parameter for the undamaged SiO_2 was found to be 0.5028 (or 0.9882) by fitting the data.

iv) S Parameter of the Interface

It was necessary to introduce into the model an interfacial region with a different S parameter. This is the only way to produce the dip in the data obtained from the unimplanted samples. In the model used to fit the data, the thickness of the interface region was 50 Å. Since the interface is so thin there is no situation in which most of the positrons annihilate at the interface. The S parameter of the SiO_2/Si interface can, however, be obtained by fitting the data. It was impossible to use a common S value for the interface of all the measurements. The S parameter value of the interface was 0.4831 (or 0.9495) for most models, but was 0.4760 (or 0.9355) after the seventh etch and 0.4680 (or 0.9198) after the eighth etch.

This effect was not observed in the implanted sample because in this case, the S parameter of the interface lies in between the S parameters of the

silicon and the damaged SiO_2 layer. For the implanted samples, it was impossible to determine the S parameter of the interface unambiguously, due to the interdependence of the data with the position of the interface. Having an S parameter for the interface that is too low can be compensated by also having the position of the interface too deep. All the fitting was done assuming that the S parameter of the interface was the same as that determined for the unimplanted samples (0.4831 or 0.9495)

v) S Parameter of Damaged SiO_2

Figure 3.1 shows the S vs. E curves for thermally grown SiO_2 on Si as grown and implanted with 10^{12}, 10^{13} and 10^{14} Si^+/cm^2. In the region ~5 keV, there are 3 possible annihilation states: the surface, the SiO_2 and damaged SiO_2. In this region the S parameter is almost constant. The S parameter of a defect in SiO_2 was determined by assuming that saturation of positron trapping occurred in the sample implanted with 10^{14} Si^+/cm^2. The S parameter used for a defects in SiO_2 was 0.4500 (or 0.8844).

vi) S Parameter of Damaged Silicon

Previous studies have shown that the defects produced by ion implantation of silicon are predominantly divacancies and that their S parameter is about 1.04 times the S parameter of bulk silicon [17,18]. This is the value used in this study.

e) Defect Distribution

The defect distribution obtained from the fitting procedure is shown in figure 4.2. The defect concentration is almost constant throughout the SiO_2 region. This defect distribution was obtained assuming that the defects have a specific trapping rate of 10^{15} s^{-1} [19].

The relative importance of the nuclear and the electronic stopping can be determined by fitting the obtained defect distribution to equation 10. The values of the fitting parameters are a = 0.22 and b = 3.704×10^{-4} defects/eV This means 1) that the amount of energy necessary to produce defects by ionization would be ~2700 eV/defect and 2) that only 22% of the defects produced by the nuclear stopping remain after recombination of defects. The energy necessary to produce a defect by ionization is comparable to the energy necessary to produce a defect by X-ray radiation which Wilson et. al. found to be ~6300 eV/defect by measuring the electronic properties of IGFETs [14]. The difference may be due to the large uncertainty in the specific trapping rate of the defects, that the 2 techniques measure different types of defects and different types of ionizing radiation were used.

The defect distribution within the silicon substrate was found to have the same shape as the vacancy distribution predicted by TRIM. Surprisingly, the value for the obtained defect concentration was different after the entire SiO_2 layer

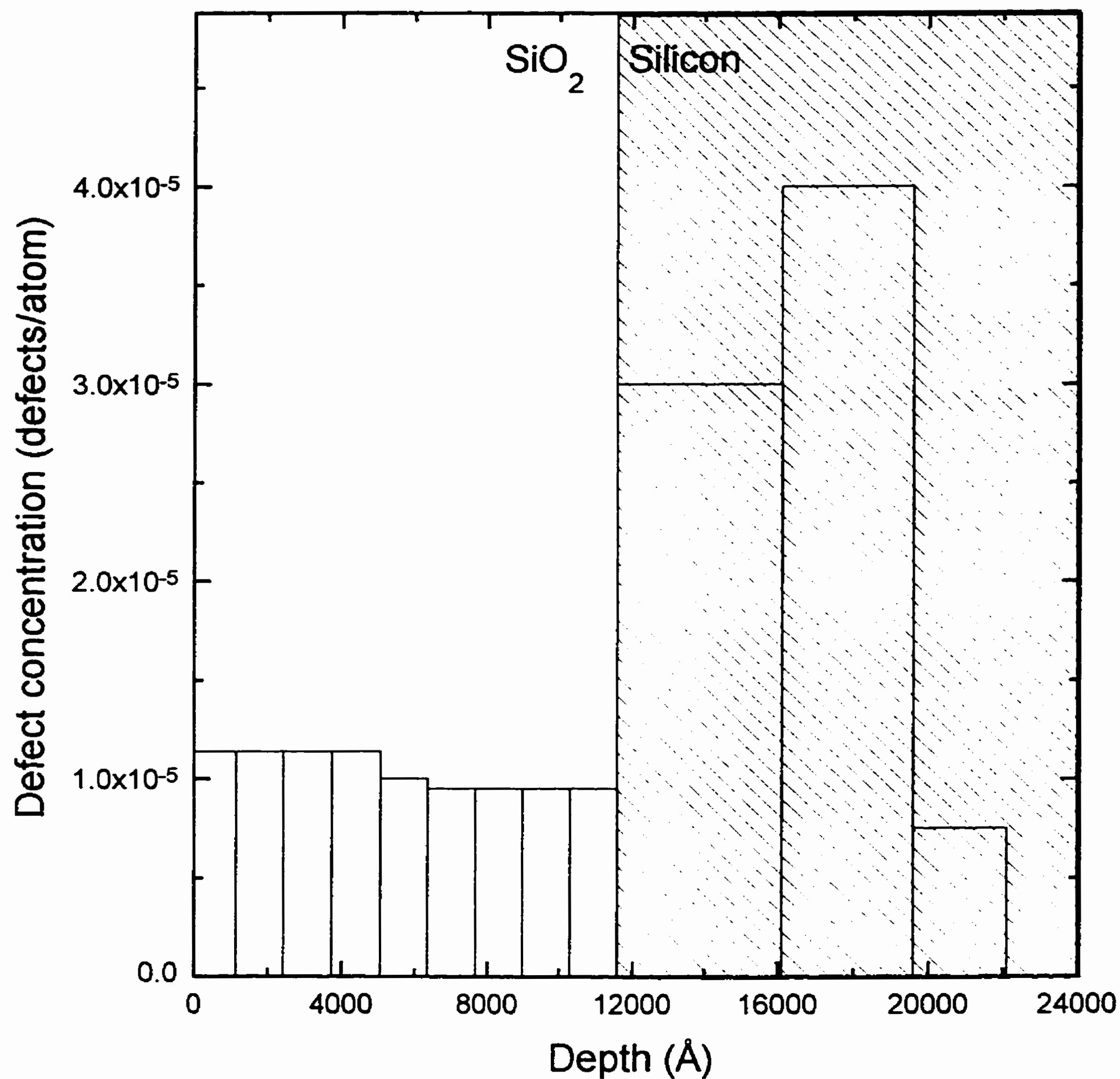

Figure 4.2 . Defect distribution obtained from the fitting of the positron annihilation spectroscopy data.

was removed. After the removal of the oxide layer the defect concentration necessary to fit the data was about 2 times higher than when the oxide layer was present.

f) Uncertainty of Defect Distribution

The uncertainty in the defect concentration was determined as the range in which the value can be changed and still give an adequate fit to the data. This gave the relative uncertainty which is about 10% for the defect concentration in each region. The absolute uncertainty in the defect concentration is much larger, since it is only possible to determine the product of the defect concentration with the specific trapping rate, and that there is a large uncertainty in the value of the specific trapping rate. It is not unlikely that the specific trapping rate is inaccurate since we do not know the defect species or its charge state. The value obtained for the defect concentration should be considered accurate to within an order of magnitude.

Chapter 5 Discussion

1. Types of Defects

There are many different types of defects produced by ion implantation of SiO_2 [20] . The normal bonding arrangement in SiO_2 is that each silicon atom is bonded with 4 oxygen atoms and each oxygen atom is bonded with 2 silicon atoms ($\equiv$Si-O-Si$\equiv$, where the " $\equiv$ " represents bonding with 3 oxygen atoms). While the predominant type of defect is the E' center ($\equiv Si^{+}$) this is not likely to be a positron trapping defect due to its positive charge. The positron trapping defects would be either neutral or negatively charged. The defects responsible for positron trapping are likely the nonbridging-oxygen hole center ($\equiv Si\text{-}O^{-}$) or the peroxy radical ($\equiv Si\text{-}O\text{-}O^{-}$) [21].

The defects produced by the electronic stopping are not necessarily the same defects as those produced by the nuclear stopping. The defect distribution was obtained assuming that there was only one type of defect. Each defect type should have its own specific trapping rate and S parameter. By assuming one value for all types of defects, the defects concentration found by the fitting procedure is only an effective defect concentration.

2. Inadequacies of the Fitting Procedure

It was impossible to fit the data using a consistent value for the S parameter of the interface. The only reason that the S parameter of the interface could

change is if there were some change in the interface. It is also possible that the model used to fit the data doesn't accurately predict the fraction of positrons annihilating at the interface.

To test whether there is a change in the interface caused by the chemical etching we compared an SiO_2 film grown to 1250 Å with a SiO_2 film etched down to 1250 Å. Although it was not possible to fit these data, the S vs. E curves are very similar indicating that there are no radical changes in the interface.

It is possible that the model does not correctly predict the fraction of positrons annihilating at the interface. The possible deficiency in the model is that the interface was modeled by a 50 Å layer with a high concentration of defects. The value of the defect concentration was 0.01 defects/atom and so should be high enough to ensure that all the positrons that enter the layer are trapped, and unable to diffuse through it.

The thickness of the interface was also chosen to be thick enough to ensure that the positrons could not diffuse through it, but thin enough that only a small fraction of positrons are implanted into it. Varying the thickness of the interface has an effect on the fraction of positrons annihilating in it, and thus has an effect on the S parameter of the interface. Other values of the

thickness of the interface were attempted but it was still impossible to find a consistent value for the S parameter of the interface.

Of the other input parameters used to model the data, the positron diffusion constant in the SiO_2 has a large uncertainty to it and may be the cause of this uncertainty. Other values for this diffusion constant were tried and none of them corrected this inconsistency. The positron diffusion constant in SiO_2 used in the model was 0.01 . This was based on an assumed free annihilation rate of $4.55x10^9$ s^{-1} and a positron diffusion length of 15 nm.

It may be that the model can not reproduce the data due to uncertainties associated with scattering from interfaces in layered structures [22,23]. Therefore, the fraction of positrons annihilating at the interface would not be calculated properly by POSTRAP5. The interface is possibly an efficient trap for even the epithermal positrons (positrons with energies higher than kT) .

Another inconsistency in the fitting is the defect concentration in the silicon substrate. For all the implanted samples the same defect distribution was used, but after all the SiO_2 was removed it was necessary to use about 2 times as many defects in the silicon. The shape of the defect distribution remained the same. This may be another effect of the interface. If epithermal positrons were scattered by the interface, then the fraction of positrons

annihilating at the interface would be different and the amount transmitted through the interface would also be different.

Chapter 6 Conclusions

The defect concentration produced by ion implantation was measured using positron annihilation spectroscopy. The chemical etching of the sample made it possible to determine the defect distribution with better depth resolution than in any previous positron study. It was found that the implantation of 1.7 MeV silicon ions produces a nearly constant defect distribution within the silicon oxide layer. Therefore, we conclude that the nuclear and electronic stopping must both play important roles in defect production in SiO_2.

It was found that 22% of the defects produced by the nuclear stopping remained after the recombination of defects and that the energy required to produce defects by ionization is 2700 eV/defect.

The defect distribution in the silicon substrate is consistent with the shape of the vacancy distribution predicted by TRIM. It has been shown that defects in silicon can be detected through an SiO_2 film as thick as 530 nm.

It was not possible to fit all the data using a consistent model. The S parameter of the interface was inconsistent for 2 of the measurements, and the concentration of defects in the silicon substrate had to be doubled after the SiO_2 was removed. These inconsistencies may be due to scattering from

the interface or due to trapping of epithermal positrons which are not considered in the model.

Future Work

Future work should include further investigations of the role of the electronic stopping in defect production. The assumption that the number of defects due to the electronic stopping is proportional to the energy loss by ionization should be verified. This can be done by varying the ion species and/or implantation

energy, which would vary the relative contributions of the electronic and nuclear stopping.

Since the defect production by the nuclear stopping is well understood, it should be informative to study situations where the damage is produced only by ionizing radiation. This can be done by irradiating SiO_2 samples with x-rays, γ-rays or electrons.

References

[1] K. Nikawa, Microelectronics and Reliability, **32** (11), 1589 (1992).

[2] E. Vincent, S. Bruyere, C. Papadas and P. Mortini, Microelectronics and Reliability, **37** (10-11) 1499 (1997).

[3] S. Q. Hong, T. Wetteroth, H. Shin, S. R. Wilson, D. Werho, T.-C. Lee and D. K. Schroder, Appl. Phys. Lett. **71** 3397 (1997).

[4] P. J. Simpson, M. Vos, I. V. Mitchell , C. Wu, P. J. Schultz, Phys. Rev. B 44, 12180 (1991).

[5] P. J. Schultz, G. R. Massoumi and W. N. Lennard, Nucl. Instr. Meth. **B90** 567 (1994).

[6] A. P. Knights, P. J. Simpson, L. B. Allard, J. L. Brebner and J. Albert, J. Appl. Phys. **79**, 9022 (1996).

[7] J. F. Ziegler, J. P. Biersack, and U. Littmark, *The Stopping and Range of Ions in Solids* (Pergamon, New York,1985).

[8] I. K. MacKenzie, C. W. Shulte, T. Jackman, J. L. Campbell, Phys. Rev. **A7**, 135 (1973).

[9] S. Valkealathi, and R. M. Nieminen, Appl. Phys. A 32, 51 (1984).

[10] A. P. Jr. Mills, R. Wilson, Phys. Rev. **A26**, 490 (1982).

[11] P. J. Schultz, and K. G. Lynn Rev. Mod. Phys., 60, 701 (1988).

[12] P. Asoka-Kumar, K. G, Lynn and D. O. Welsh, J. Appl. Phys. 76 (9) 4935 (1994).

[13] H. Nishikawa, R. Nakamura, R. Tohmon, Y. Ohki, Y. Sakurai, K. Nagasawa, Y. Hama, Phys. Rev. B 41, 7828 (1989).

[14] C. K. Williams, A. Reisman, P. Bhattacharya, and W. Ng, J. Appl. Phys 64, 1145 (1988).

[15] U. Myler and P. J. Simpson, Phys. Rev. **B56**, 14303 (1997).

[16] G. C. Aers, in *Positron Beams for Solids and Surfaces*, The Proceedings of the Fourth International Workshop, edited by P. J. Shultz, G. R. Massoumi and P. J. Simpson, AIP Conference Proceedings 218 (AIP, New York, 1991).

[17] Keinonen, Phys Rev. **B37**, 8269 (1988).

[18] A. Uedono, S. Tanigawa, J. Sugiura, and M. Ogasawa , Jpn. J. Appl. Phys. 29, 1867 (1990).

[19] P. Mascher, S. Dannefaer and D. Kerr, Phys. Rev. **B40**, 11764 (1989).

[20] D. L. Griscom, J. Non-Chryst. Solids **73**, 51 (1985).

[21] M. Fujinami and N. B. Chilton, Appl. Phys. Lett. **62**, 1131 (1993).

[22] V. J. Ghosh, Appl. Surface Sci. **85**, 187 (1995).

[23] G. C. Aers, P. A. Marshall, T. C. Leung, and R. D Goldberg, Appl. Surface Sci. **85**, 196 (1995).

IMAGE EVALUATION TEST TARGET (QA-3)

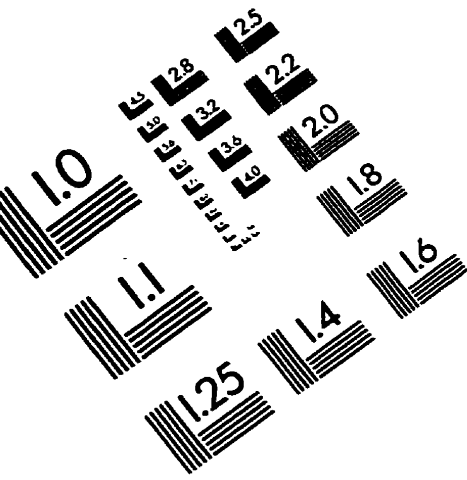
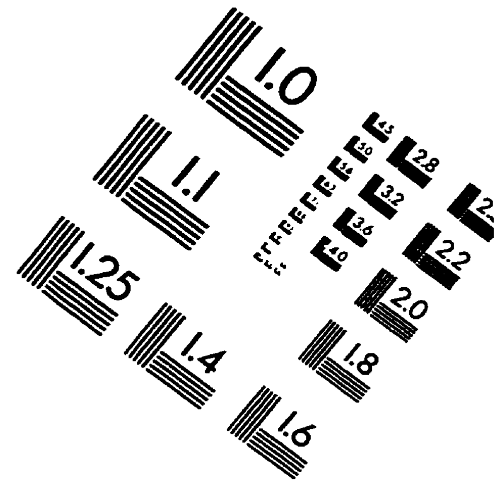
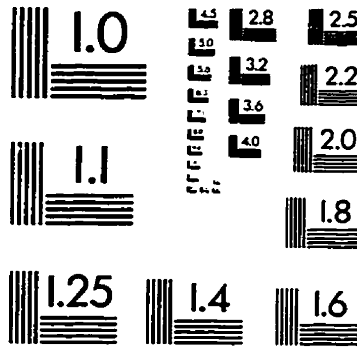
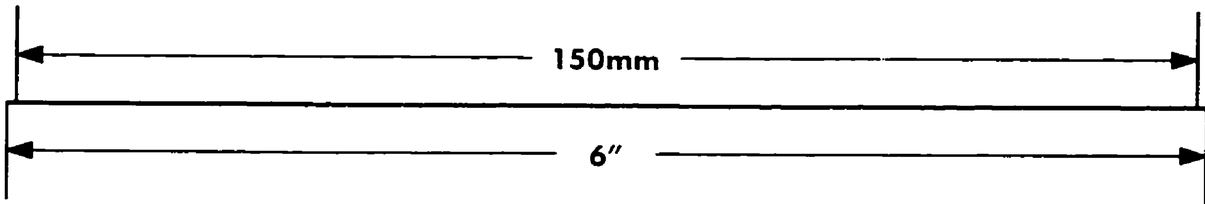

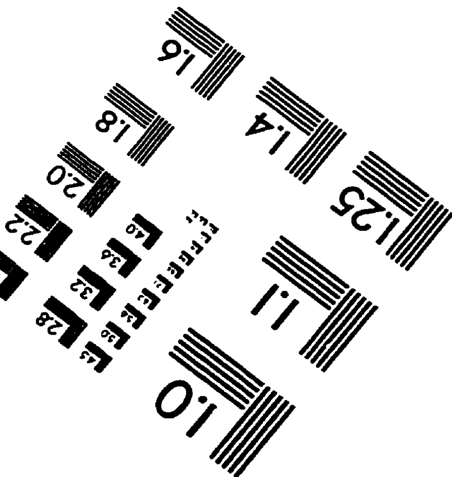

APPLIED IMAGE . Inc
1653 East Main Street
Rochester, NY 14609 USA
Phone: 716/482-0300
Fax: 716/288-5989

© 1993, Applied Image, Inc., All Rights Reserved